GEOMETRICAL CHARACTERIZATION OF THE CORONARY ARTERIAL TREE

Carlos A. Bulant[1,2,*]

Pablo J. Blanco[1,2]

Antonildes N. Assunção Jr.[3]

Gabriela Liberato[3]

Thais Pinheiro Lima[3]

José R. Parga Filho[3]

Pedro A. Lemos[3]

Luiz F. Rodrigues de Ávila[3]

Raúl A. Feijóo[1,2]

[1] Laboratório Nacional de Computação Científica

Av. Getúlio Vargas 333, 25651-075, Petrópolis, Rio de Janeiro, Brazil

[2] Instituto Nacional de Ciência e Tecnologia em Medicina Assistida por Computação Científica (INCT/MACC)

Av. Getúlio Vargas 333, 25651-075, Petrópolis, Rio de Janeiro, Brazil

[3] Instituto do Coração da Faculdade de Medicina da Universidade de São Paulo (InCor-HC/FMUSP)

Av. Dr. Enéas de Carvalho Aguiar 44, 05403-000, São Paulo, Brazil

[*] bulant@lncc.br

Abstract. *In this work we present a computational aided work-flow for the geometric characterization of coronary arterial networks obtained from non-invasive computed tomography angiography (CTA). Arterial structures are segmented from CTA images using a semi-automated pipeline based on a Level-Set technique. After surface improvement, the arterial tree backbone is modeled with polylines containing point-wise information, on top of geometric objects called centerlines, which are composed in a graph-like structure that accounts for the coronary arterial anatomy. Coronary tree models are then characterized in terms of geometric features,*

which provide information for individual segments, bifurcations and, ultimately the complete network. Labeling of arterial segments and the identification of lesions severity is carried out by specialized professionals. As a proof of concept we present preliminary data analysis for arterial morphometrics and geometrical comparison.

Keywords: *Arterial centerline, Geometric features, Arterial comparison, Coronary tree.*

1 INTRODUCTION

According to Roth et al. (2015), cardiovascular diseases (CVD) are the leading cause of deaths worldwide. Among them, coronary heart disease is the leading one. Although CVD usually affects older adults, the antecedents of cardiovascular disease, notably atherosclerosis, begin in early life, making primary prevention efforts necessary from childhood (McGill et al., 2008). Therefore, there is increased emphasis on preventing atherosclerosis by tackling systemic risk factors, such as healthy eating, exercise, and avoidance of smoking. Nonetheless, other risk factors are known, namely, (i) studies suggest a connection between CVD with hereditary factors (Fischer et al., 2007); (ii) the notion that biomechanics (shear stress produced by blood flow) is involved in the atherosclerotic process (Thubrikar and Robicsek, 1995) is by now widely accepted, however, to date the precise mechanism behind the disease remains unknown; (iii) geometrical risk factors had been focus of research since the early 80's (Friedman et al., 1983).

Due to their asymptomatic nature, most CVD are detected in an advance developed state. Furthermore, the detection and diagnosis of CVD would be extremely difficult without medical imaging techniques such as angiography (AX), computed tomography angiography (CTA, or simply CT), magnetic resonance angiography (MRA) or intra-vascular ultrasound (IVUS), among others. For the particular case of coronary artery disease (CAD), invasive angiography has long been considered the "gold standard". However but multi-slice CTA (MSCTA) is gaining popularity among cardiologist as the new gold standard (Sun, 2010).

Image segmentation of MSCT can provide accurate three-dimensional models of complete coronary trees (at the arterial level), which can be further characterized in terms of geometrical features of arteries and stenosis. In turn, the analysis of these geometric features and their relation to arterial lesions are the essence behind the so called geometric risk factors (Friedman et al., 1983). To prove such hypothesis, it is required to process a large quantity of patients, followed by the application of data mining techniques to identify connections between features and disease.

The previous is the context in which the present work is framed, specifically, we propose a computational aided work-flow for the geometric and morphological characterization and analysis of coronary arteries, obtained from non-invasive CTA images. The computational framework here presented provides the basis for future assessment of geometric risk factors. The remaining of this document is organized as follows. Section 2 overviews the general work-flow. Details on the image segmentation and processing pipeline are presented in Section 2.1. The mechanisms adopted to model and characterize coronary trees is explained in Section 2.3. Results of statistical analysis are presented in Section 3. Final remarks are outlined in Section 4.

2 METHODOLOGY

Ex-vivo anatomical characterization of coronary arterial trees from basic variables like vessel length and radius was explored by the medical community elsewhere (Dodge et al., 1992; Fiss, 2007; Ballesteros and Ramirez, 2008; Loukas et al., 2009), and it is basic knowledge for cardiology students, physicians and surgeons. Advances on medical imaging and processing tools allow further characterization from in-vivo data extracted from AX images (Zhu et al., 2009). Nevertheless, using AX images implies invasive medical procedure and the use of a rather incomplete anatomic characterization. To the best of our knowledge, complete coronary trees have not been geometrically characterized from in-vivo images. Some studies tried to relate arterial geometry to disease, for example Dvir et al. (2003) found that C-shaped right coronary arteries (RCA) are more prone to develop stenosis than Σ-shaped started; Ikeda et al. (1991) found that wider bifurcation angles are related to stenosis in young adults. Bogunovic (2012) explored the characterization and classification of carotid arteries[1], using a set of standard features, i.e. length, tortuosity, radii, curvature, torsion, etc. He also used the large deformation diffeomorphic metric curve mapping (LDDMCM) (Glaunès et al., 2008), to provide correspondences between centerlines and to define a metric in shape space. We propose a similar methodology to study coronary trees, using more geometric features and characterizing a set of arteries instead of a single one.

A relational database was designed and implemented to storage all heterogeneous data entered to, and generated by each step of the work-flow. The proposed methodology is illustrated in Fig. 1 and consists of five steps: (i) Input of medical data, including patient, study and image information; (ii) Medical image processing (see Section 2.1), the output of this step is an *initial mesh* of the arterial structures, i.e. a triangulation of the surface that stands for the boundary of the arterial lumen; (iii) Generation of geometric models, based on *centerlines* (see Section 2.3), the *initial mesh* is refined and centerline information is extracted. The basic processing of *centerlines* includes arterial labeling (performed by specialized cardiologist) and bifurcation detection; (iv) Geometrical and anatomical characterization of centerlines yielding a variety of descriptors that are store into the database; (v) Data mining and analysis performed over the database.

It is noteworthy that image processing activities described in Section 2.1 are performed using vmtk[2] and ImageLab[3] softwares, while mesh processing and centerline extraction (Section 2.2) are performed using vmtk and HeMoLab[3].

2.1 IMAGE SEGMENTATION AND PROCESSING

Patient specific arterial geometries are obtained from CTA image segmentation. A methodology previously presented in Bulant (2013), based on Antiga et al. (2008), was refined and tuned to be used on the coronary arterial network. The proposed segmentation pipeline is based on implicit deformable models, which in the context of this work means a deformable surface $S(t) : \mathbb{R}^2 \times \mathbb{R}^+ \rightarrow \mathbb{R}^3$ described through the iso surface of the scalar function $\phi(\mathbf{x}, t) : \mathbb{R}^3 \times \mathbb{R}^+ \rightarrow \mathbb{R}$, such that $S(t) = \{\mathbf{x}, \phi(\mathbf{x}, t) = 0\}$. The technique used to calculate the temporal evolution of $S(t)$ is known as Level-Set, and the model for this evolution is described by a

[1] Largest arteries in the neck, that provide the major blood supply to the head.

[2] `www.vtmk.org`

[3] `www.lncc.br/prjhemo/`

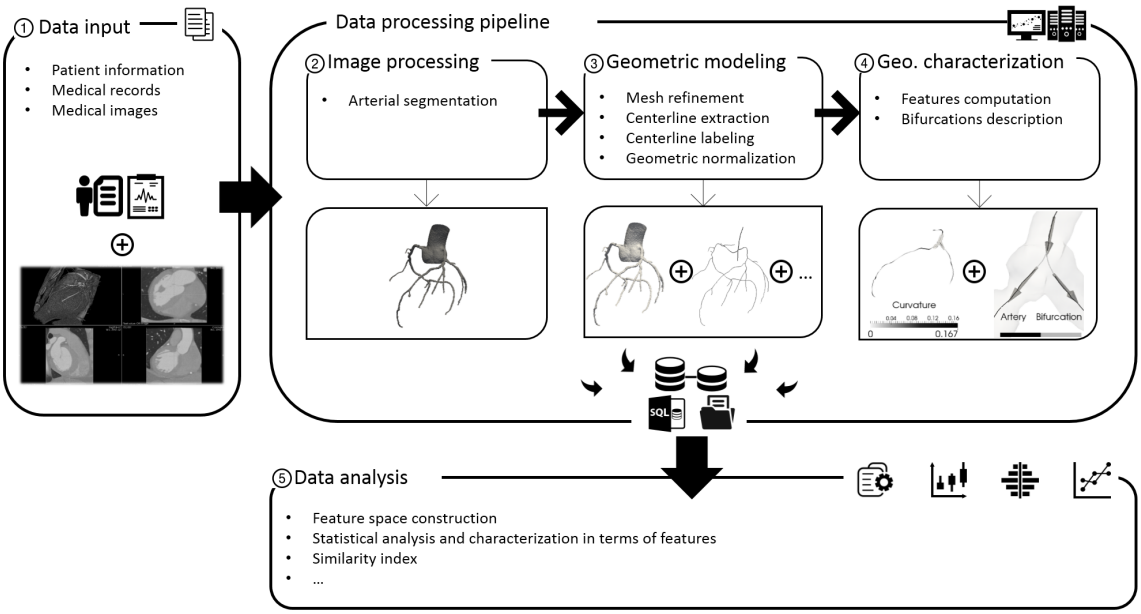

Figure 1: Illustration of the proposed general work-flow.

minimization process of a cost functional for which the associated partial differential equation is

$$\frac{\partial \phi}{\partial t} = -w_p P(\mathbf{x})|\nabla\phi| + 2w_k K(\mathbf{x})\kappa(\mathbf{x})|\nabla\phi| - w_a \nabla A(\mathbf{x}) \cdot \nabla\phi, \tag{1}$$

where the first term on the right-hand side represents surface inflation with a position-dependent speed given by $P(\mathbf{x})$, which can depend on image features or on shape constraints; the second term represents a smoothness constraint on the surface, being $\kappa(\mathbf{x}) = \operatorname{div} \frac{\nabla\phi}{|\nabla\phi|}$ the mean curvature of the zero-level surface restricted to the spatial modifier $K(\mathbf{x})$; and the last term represents advection of the surface by means of the given vector field $\nabla A(\mathbf{x})$. Weights w_p, w_k and w_a regulate the influence of each term on surface evolution.

In order to solve Eq. (1), an initial solution must be given, which is obtain by a semi-automated procedure: For each arterial segment, (i) the user manually places two seeds, one at the beginning and the other at the end of the segment; (ii) The colliding front method (Antiga et al., 2008) is used to obtain an initial segmentation of the vessel, which is a binary image differencing the arterial lumen from the rest of the domain; (iii) The output of the colliding front procedure is used as initial guess for the solution of the Level-Set equation.

The complete segmentation pipeline is illustrated in Fig. 2 and is done by performing five operations: (i) Region Of Interest (ROI) extraction; (ii) Standard curvature anisotropic filtering, according to Whitaker and Xue (2001), is performed when the images present high levels of noise. Typical parameters values are 10 iteration, a time step of 0.0625 and conductance of 4. (iii) Interactive initialization of individual arteries using colliding fronts; (iv) Numerical approximation of the Level-Set equation, in which, for this work, the mean and standard deviation of parameters were: $w_p = 0.64 \pm 0.24$, $w_k = 0.59 \pm 0.20$, $w_a = 0.97 \pm 0.16$ and the number of iteration 108 ± 44. These parameters depend on image quality and arterial characteristics, for example noisy images are better segmented with higher values of w_k and more iterations, while

small arteries are better defined with higher values of w_p. Arterial regions with conventional stents are challenging, and require more user interaction during initialization and lower values of w_p. Finally, (v) construction of surface mesh using the marching cubes method (Lorensen and Cline, 1987). Figure 3(a) presents some examples of coronary arterial trees segmentations for different patients.

As a general rule, the aortic root and all visible arteries are segmented. Depending on image quality and patient anatomy the number of arterial structures varies from study to study (20 ± 6). A total of 54 patients were segmented and included in this study.

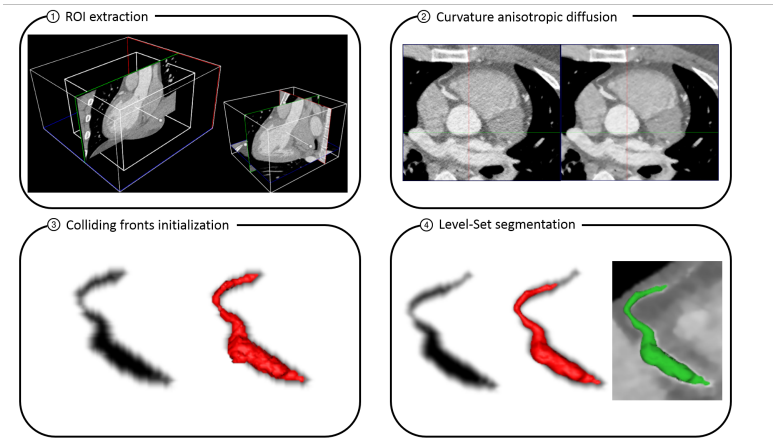

Figure 2: Illustration of the image segmentation pipeline: (1) extraction of the region of interest; (2) curvature anisotropic diffusion filter that smooths out image noise; (3) colliding front method as the resulting binary scalar field and associated implicit surface for the proximal portion of a right coronary artery; (4) the Level-Set scalar field and zero-level surface.

2.2 Mesh processing and centerline computation

After image segmentation, surface meshes are clipped at all arterial endpoints, disconnected regions (if any) are deleted, and surface smoothing is performed. The resulting mesh is used for centerline computation as explained by Antiga et al. (2003). The characterization of arterial structures from centerlines is a widely used approach (O'Flynn et al., 2007; Meng et al., 2008; Zhu et al., 2009; Piccinelli et al., 2009; Bogunovic, 2012; Wright et al., 2013; Mut et al., 2014). Three-dimensional centerlines are represented as polylines with point-wise information (e.g. lumen radius), which admits classic differential geometry analysis to compute, for example, point-wise curvature and torsion. The first process performed over the centerlines is the detection of arterial tracks, which are polylines elements between bifurcation points. Then, these arterial segments are manually labeled by a cardiologist using the HeMoLab software, and vessels with same label are merged to model complete arteries, see Fig. 3(b). Labeling is key for correct data storage, future statistical analysis and comparison of arterial structures. Cardiologists also report which arteries suffer from lesions and characterize them according to Table 1.

Bifurcation regions over the centerline are detected and masked using a procedure explained in Piccinelli et al. (2009). Bifurcation vectors are then computed for the parent artery (in-vector) and the branches (out-vectors), see Fig. 3(c). The out-vectors are computed by taking as origin the point at which the bifurcation mask ends, and as end point the weighted mean

of N successive points[4], where weights are computed as $(N-i)^{-1}$, being $i \in [1, N]$ the index of the point.

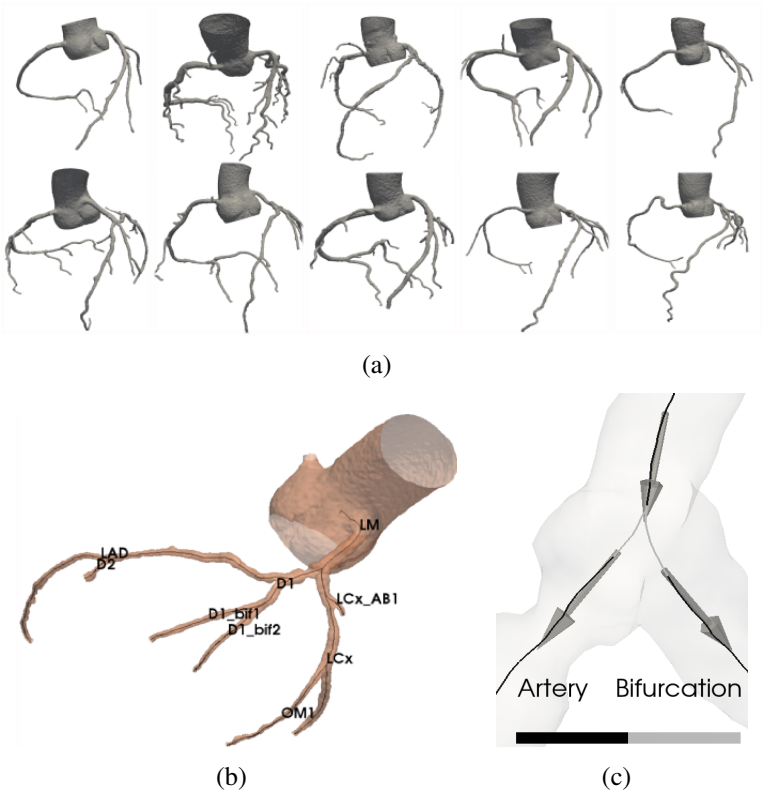

(a) (b) (c)

Figure 3: Panel (a) presents examples of coronary tree meshes after processing operations. Panel (b) shows labeled centerline of a left coronary tree. Panel (c) shows bifurcation masks and vectors over a centerline.

Table 1: Stenosis characterization parameters used by cardiologists to describe lesions on arteries.

Stenosis grading	**Tissue type**	**Lesion position**
Normal	Soft tissue	Proximal
Mild: 25% - 49%	Calcification	Medium
Moderate: 50% - 69%	Mixed	Distal
Severe: 70% - 99%		
Occluded		

2.3 Coronary tree characterization and comparison

At this point, patient specific coronary tree models can be geometrically described by a set of features. For each artery A, the following descriptors are computed

- **Branch count** (Υ): The number of arteries (in the centerline model) branching from A.

[4]In this work, $N = 10$, if the arterial segment has less than 10 points after bifurcation mask ended, the remainder point are extrapolated in the direction of the last two points.

- **Parent**: The label of the artery that gives rise to *A* according to the network topology. In some pathological cases, the coronary tree deviates from its normal topology, for example the left circumflex (LCx) and the left anterior descendant (LAD) may rise directly from the aorta (Ao) in patients with absence of left main artery (LM).
- **Length** (ℓ): The arc length of the curve described by *A*.
- **Tortuosity** (χ): The relative increment in the length of a curve deviating from a straight line (Piccinelli et al., 2009), which is computed as

$$\chi = \frac{\ell}{d} - 1, \tag{2}$$

where d is the euclidean distance between the start and end point of A. The tortuosity defined in (2) has a minimum value (zero) when the vessel is straight, and increases when *A* is more tortuous.

- **Radius** (r): The arterial radii, which is a point-wise variable defined along the *centerline abscissa* $s \in [0, \ell]$, the *minimum* (r_m), *maximum* (r_M) and *mean* ($\bar{r}$) values are then computed.
- **Curvature** (κ): Measures the deviation of the curve from a straight line (zero curvature). The Frenet–Serret theory of differential geometry provides the standard definition of curvature as

$$\kappa(s) = \frac{|\mathbf{c}'(s) \times \mathbf{c}''(s)|}{|\mathbf{c}'(s)|^3}, \tag{3}$$

where $\mathbf{c}(s)$ is the centerline curve parametrized with the *curvilinear abscissa*, and $(\cdot)'$ indicates the derivative operator. As κ is defined for each point along the centerline, the *minimum* (κ_m), *maximum* (κ_M), *mean* ($\bar{\kappa}$) and *total* (κ_T, integral of the curvature in over the centerline) values are computed.

- **Torsion** (τ): Measures the curve local deviation from lying on the osculating plane, or equivalently, how sharply the line is twisting in space. The standard definition of torsion is

$$\tau(s) = \frac{|(\mathbf{c}'(s) \times \mathbf{c}''(s)) \cdot \mathbf{c}'''(s)|}{|\mathbf{c}'(s) \times \mathbf{c}''(s)|^2}. \tag{4}$$

Analogous to curvature, the torsion is defined for each point along the centerline, therefore the *minimum* (τ_m), *maximum* (τ_M), *mean* ($\bar{\tau}$) and *total* (τ_T) values are computed.

- **Combined curvature** (ζ): Accounts for curvature and torsion at each point of the curve O'Flynn et al. (2007), and is calculated according to

$$\zeta(s) = \sqrt{\kappa(s)^2 + \tau(s)^2}. \tag{5}$$

As in the case of other point-wise defined variables, the *minimum* (ζ_m), *maximum* (ζ_M), *mean* ($\bar{\zeta}$) and *total* (ζ_T) values are computed.

- **Aspect ratio** (Λ_r): Accounts for the relationship between the arterial length and the *mean radius* (Mut et al., 2014),

$$\Lambda_r = \frac{\ell}{\bar{r}}. \tag{6}$$

- **Curvature ratio** (Λ_κ): Dimensionless ratio of vessel radius with curvature defined by Bogunovic (2012), assuming that the polyline modeling the curve has N points, the discrete definition of the curvature ratio is

$$\Lambda_\kappa = \frac{1}{N}\sum_{i=1}^{N} \kappa_i^2 r_i^2 \,. \tag{7}$$

- **Torsion ratio** (Λ_τ): Defined as the mean product between torsion and radius along the centerline, defined by Bogunovic (2012), its discrete form is

$$\Lambda_\tau = \frac{1}{N}\sum_{i=1}^{N} \tau_i^2 r_i^2 \,. \tag{8}$$

- **Bending energy** (ξ_κ): Defined as the energy needed to bend an straight line into its curved shape (Meng et al., 2008). It corresponds to the average value of the square curvature scaled by the total arc length of the centerline under analysis, the discrete form is

$$\xi_\kappa = \frac{\ell^2}{N}\sum_{i=1}^{N} \kappa_i^2 \,. \tag{9}$$

  The ℓ^2 factor guarantees scale invariance (i.e., any circle will always have the same energy value), is required for comparisons between curves with different lengths.

- **Twisting energy** (ξ_τ): Is the energy needed to twist an straight line into its curved shape (Meng et al., 2008), the discrete form is

$$\xi_\tau = \frac{\ell^2}{N}\sum_{i=1}^{N} \tau_i^2 \,. \tag{10}$$

- **Fractal dimension** (ϱ): Defined by Wright et al. (2013) as the slope of the linear regression obtained from the log-log scatter plot of length vs. euclidean distance, moving from the second to the last point along centerline.

- **Rising angle** (α): The angle between the artery *A* and its parent. It is computed over the plane formed by the bifurcation vectors, using the well known formula

$$\alpha = \arccos(\mathbf{v}\cdot\mathbf{w}) \,, \tag{11}$$

  where $\mathbf{v}$ is the parent artery vector indicating the direction towards the branch and $\mathbf{w}$ the vector indicating the rising direction of *A*.

- **Offspring mean raising angle** (β): Given the artery *A*, the mean of α over the offspring of *A* is computed.

- **Lesions count** (η): A list of arterial lesions defined by quantities described in Table 1 is produced for each arterial segment, based on clinical data. From this list, the quantity of lesions is easily obtained.

It is worth noting that computation of curvature and torsion are performed using finite differences over an smoothed polyline. This curve is constructed using a Laplacian filter to get rid of spurious high-frequency noise (Piccinelli et al., 2009). Note that this procedure is only employed for the computation of derivatives with respect to the parametric coordinate.

At this stage, each patient is modeled through the centerline of the coronary tree, and each artery is characterized by a set of real numbers (feature values). The next step consists in the construction of a mathematical environment suitable for quantitative comparisons. We propose a four-step pipeline to establish similarity between patients,

1. **Arterial selection**: A subset of arteries ($\mathcal{S}_{\mathscr{A}}$) is used to represent each patient. In this work we focus on the LAD, LCx and RCA arteries, studying them separately and all together.
2. **Feature selection**: A subset of features $\mathcal{S}_{\mathscr{F}}$ is chosen to characterize each artery. In this work we study the case when $\mathcal{S}_{\mathscr{F}}$ contains all the features.
3. **Features space construction**: Each patient is represented by a vector $\hat{\mathbf{p}} \in \mathbb{R}^n$, with $n = |\mathcal{S}_{\mathscr{A}}| \times |\mathcal{S}_{\mathscr{F}}|$. As features differ in metric units and magnitude, a normalization of each feature (dimension) is required. Given a vector $\hat{\mathbf{p}}$, the normalization is $p_f = (\hat{p}_f - \hat{\mu}_f)\hat{\sigma}_f$, $f = 1, \ldots, n$, where $\hat{\mu}_f$ is the mean value of feature f for all the patients and $\hat{\sigma}_f$ its standard deviation along the entire set. The resulting euclidean space is called *features space* and is denoted as $\mathscr{F}$.
4. **Features space elements**: Each patient is normalized and its vector representation in $\mathscr{F}$ is computed. Once all patients are represented in the features space, distances and likelihoods between patients are straightforwardly obtained.

In this work we define likelihood through the euclidean norm (denoted by $||\cdot||$) in $\mathscr{F}$. Therefore, given two different patients $\mathbf{a}, \mathbf{b} \in \mathscr{F}$, the similarity ($\mathsf{s}$) between them is defined as

$$\mathsf{s}(\mathbf{a}, \mathbf{b}) = ||\mathbf{a} - \mathbf{b}|| \tag{12}$$

Note that $\mathsf{s} \to 0$ means proximity (likeness) between patients.

3 RESULTS

In this section we present examples of the kind of information that can be extracted from the database. Figure 4 presents the mean and standard deviation of each feature described in Section 2.3, for two of the major coronary arteries, the left anterior descending (LAD) and the left circumflex (CLx). In order to observe if the sex of the patient is related to the features, the entire sample population ($n = 54$) was divided into female ($n = 17$) and male ($n = 37$) samples. Standard two-tailed t-Student test (accounting for different variances) was performed. The goal of this test is to detect which features have, statistically significant ($p \leq 5\%$), different mean values between samples. It was found that for the LAD (Fig. 4(a)): (a) females have (in average), minimum (r_m) and mean ($\bar{r}$) radius smaller than males and the general population; (b) The torsion ratio (Λ_τ) in the female sample tends to be smaller than the males and general population; (c) The number of lesions is smaller in females than males. In contrast, the LCx (Fig. 4(b)) shows that: (d) the only feature with significant difference in mean value is the

tortuosity (χ), which is smaller in female than males and the general samples; (e) again, the number of lesions is less in the female sample than the male one.

Performing the same t-Student test to the distributions of feature values when the samples are different arteries, it can be shown that the characteristic values of descriptors vary among arteries, see Fig. 5. In this case it is easier to describe which features have no statistical significant different values: (a) The length (ℓ) between LAD and RCA; (b) the maximum radii (r_M) between LAD and LCx, which is expected, since both branch from the same vessel; (c) The minimum curvature (κ_m) between the RCA and the other two arteries; (d) The maximum and mean curvature ($\kappa_M, \bar{\kappa}$) seems to have an invariant mean among arteries; (e) The total curvature (κ_T) of the LAD and RCA seems to have similar mean; (f) The minimum torsion (τ_m) of the LAD is not different between LCx and RCA; (g) The mean torsion ($\bar{\tau}$) between the LAD and RCA does not differ in mean with statistical significance; (h) The minimum combined curvature (ζ_m) between LAD and RCA; (i) The maximum combined curvature (ζ_M) between LCx and RCA; (j) The curvature ratio (Λ_κ) between LCx and RCA; (k) The torsion ratio (Λ_τ) between the LCx and the other two arteries; (l) The bending energy between the LAD and the RCA; (m) The fractal dimension (ϱ) between the LCx and the other two arteries; (n) The rising angle (α) of the LCx and RCA; (o) The mean rising angle of the offspring (β) between the LAD and RCA; (p) The number of lesions (η) between the RCA and the other two arteries.

We now present an example showing how the similarity among patients varies according to different arterial subsets, $\mathcal{S}^a_{\mathscr{A}} = \{\text{LAD}\}$ and $\mathcal{S}^b_{\mathscr{A}} = \{\text{LAD, LCx, RCA}\}$. Figure 6 presents the centerline of the LAD artery for a randomly selected patient, **A** (black); The closest, **B** (green); The most different, **C** (red); Patient **D** (orange) the closest to **C**. It is clear to observe qualitative differences between patients, for example: **C**-**D** are shorter and straighter than **A**-**B**; The later seems to reach the apex of the heart while the former do not. When computing distances in $\mathcal{S}^b_{\mathscr{A}}$, that is including two more arteries in the space, the proximity between patients may change. Particularly, see Fig. 7, the closest patient to **A** (black) is now **E** (purple), although **C** (red) continues to be the most different to **A**, and **D** (orange) remains to be the closest to **C**. Figure 7 (top) shows how different **A** is to **C** and **D** and the similarities between these last two; while Fig. 7 (bottom) shows that the similarity between the LAD of **A** and **B** does not compensate the difference between the LCx and RCA arteries, which explains why, in $\mathcal{S}^b_{\mathscr{A}}$, patient **E** is the closest to **A**.

4 FINAL REMARKS

We presented a computational work-flow designed to extract, store and analyze coronary arterial trees from non-invasive medical images (CTA). The methodology takes into account a bast number arterial descriptors from the literature, which have not been analyzed all-together for the heart arterial network. Conventional statical analyses showed that some features have different expected values for some arteries, and that sex seems to have a little impact on geometrical feature values. It was presented that proximity between patients depend on the tree model (arterial subsets), this method for computing likelihood between patients can be use for classification and profiling.

The current study has some limitations: (i) image artifacts due to calcified plaque, stents or patient movement can introduce noise into the segmentation and therefore in the centerline model; (ii) Due to image quality and resolution, the reconstructed branches are limited in size;

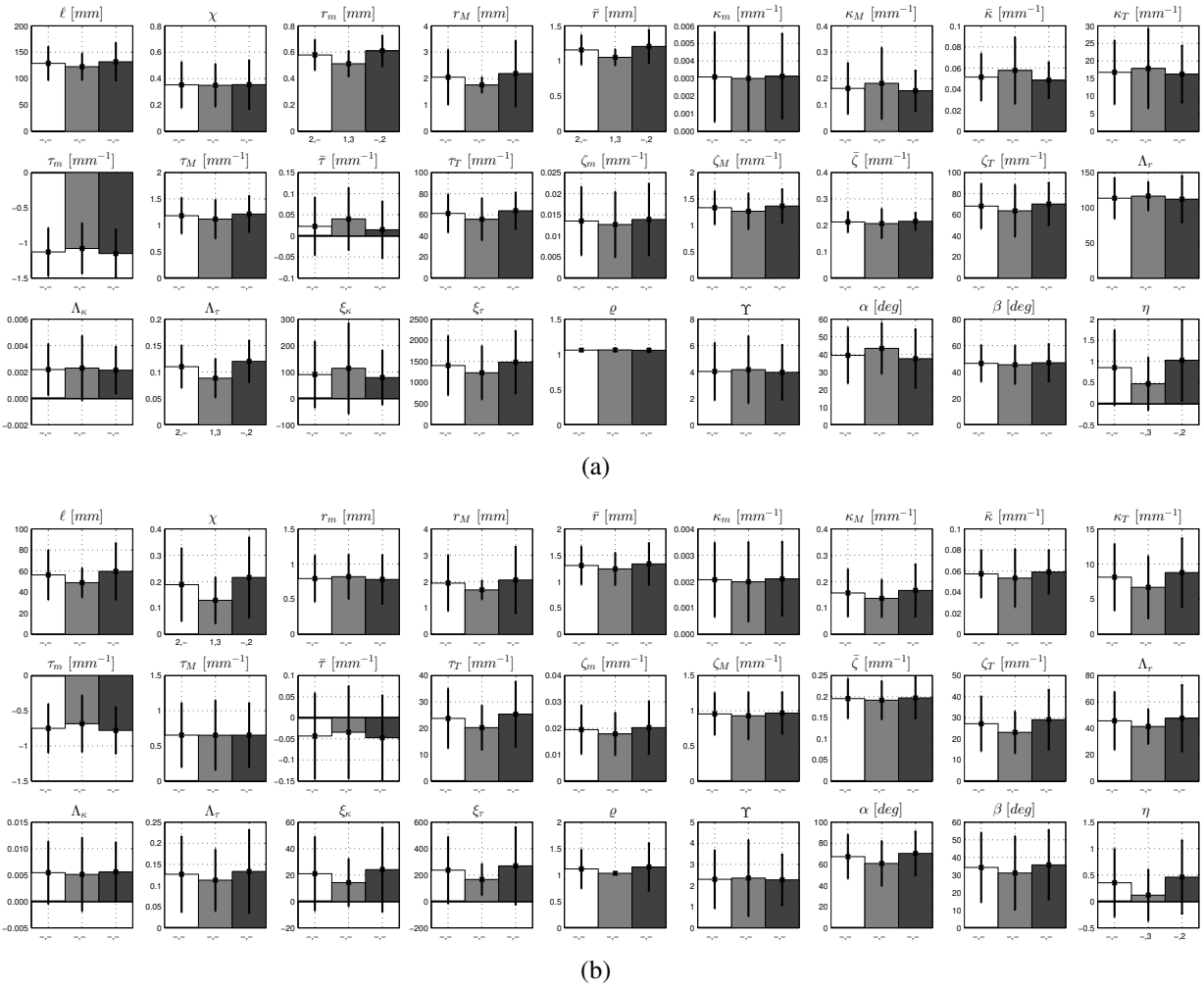

Figure 4: Mean and standard deviation per feature considering the entire sample (white, $n = 54$), female (light gray, $n = 17$) and male patients (dark gray $n = 37$). Abscissa label *i,j* under bar *k* indicates that the t-Student is statistically significant ($p < 5\%$) for samples *k,i* and *k,j*, signifying that those samples have different mean values. Panels (a) and (b) present statistics for the LAD and LCx, respectively.

(iii) Large values of the maximum radius (r_M) feature in RCA arteries are due to inaccurate bifurcation mask definition (automatically performed) for some patients, which includes in the centerline, points inside the right aortic sinus beyond the arterial ostium, which present large radius values; (iv) The arterial trees are not normalized to account myocardial size. Points (i-ii) are technological limitations, and only can be address by performing cautious segmentation and discarding images with poor quality. Point (iii) can be tackled by manual correction of the bifurcation mask in the case of branches arising from the aorta; The normalization of the centerlines models (point iv), is focus of current research. Future test will also include correlation of lesion to geometric descriptors.

ACKNOWLEDGEMENTS

This work was supported by the Brazilian agencies CNPq and FAPERJ. The support of these agencies is gratefully acknowledged.

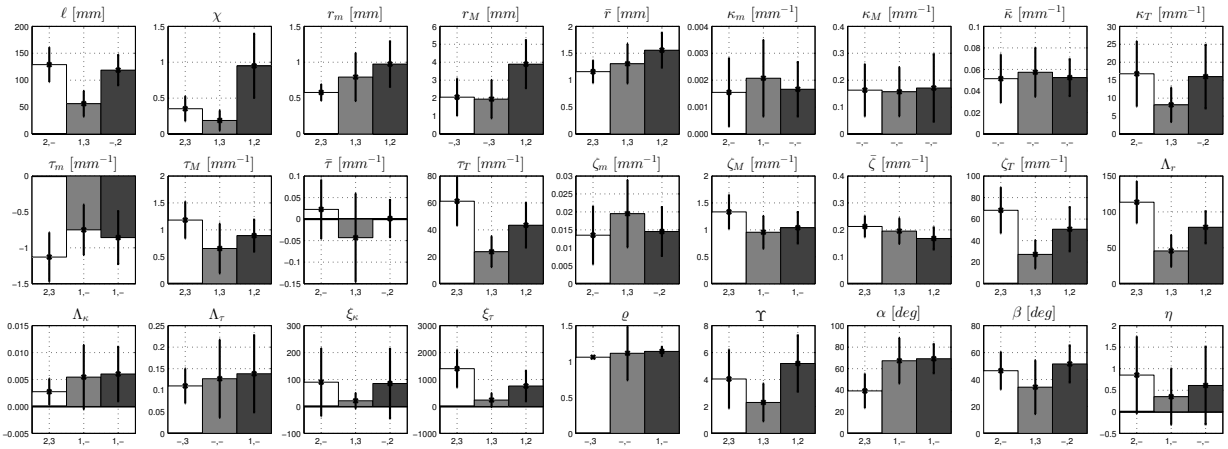

Figure 5: Mean and standard deviation per feature for the entire sample ($n = 54$), considering the LAD (white), LCx (light gray) and RCA (dark gray) arteries. Abscissa label *i,j* under bar *k* indicates that the t-Student is statistically significant ($p < 5\%$) for samples *k,i* and *k,j*, signifying that those samples have different mean values.

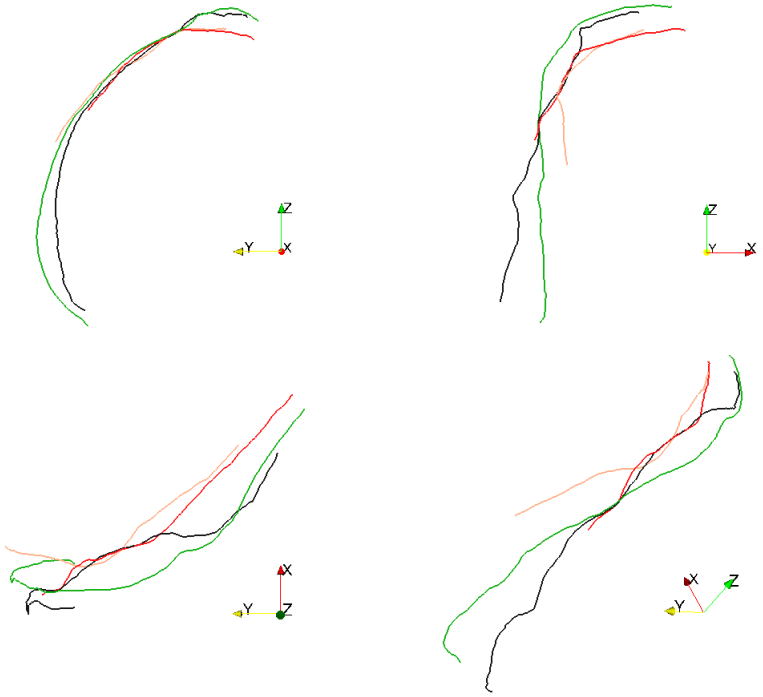

Figure 6: Visualization of the centerline for the LAD artery of four patients. A randomly selected patient, A (black); The most similar patient, B (green); the most different patient, C (red); And patient D (orange) is the most similar to C. Panels presents four different points of view of the same arteries.

REFERENCES

Antiga, L., Ene-Iordache, B., and Remuzzi, A. (2003). Computational geometry for patient-specific reconstruction and meshing of blood vessels from MR and CT angiography. *IEEE Transactions on Medical Imaging*, 22(5):674–684.

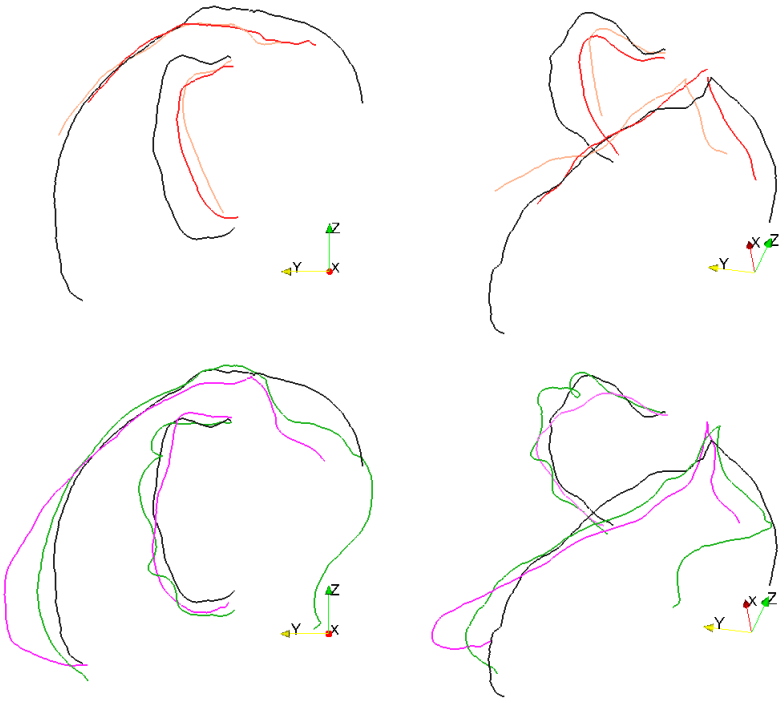

Figure 7: Visualization of the centerline for the LAD, LCx and RCA arteries of five patients. Top panels show patient A (black), the most different C (red) and the closest to C, which is patient D (orange). The bottom panels show (for the same view points) patient A (black), patient B (green) which was the closest to A when considering only the LAD, and patient E (purple) which is the closest to A when considering the three arteries.

Antiga, L., Piccinelli, M., Botti, L., Ene-Iordache, B., Remuzzi, A., and Steinman, D. A. (2008). An image-based modeling framework for patient-specific computational hemodynamics. *Medical & Biological Engineering & Computing*, 46(11):1097–1112.

Ballesteros, L. E. and Ramirez, L. M. (2008). Morphological expression of the left coronary artery: a direct anatomical study. *Folia morphologica*, 67(2):135–142. PMID: 18521813.

Bogunovic, H. (2012). *Geometric modeling and characterization of the circle of willis*. PhD thesis, Universitat Pompeu Fabra.

Bulant, C. A. (2013). Angiography image reconstruction and segmentation using variational techniques and level-set methods. Master thesis, LNCC, Av. Getúlio Vargas 333, Petrópolis, RJ, Brazil.

Dodge, J. T., Brown, B. G., Bolson, E. L., and Dodge, H. T. (1992). Lumen diameter of normal human coronary arteries. influence of age, sex, anatomic variation, and left ventricular hypertrophy or dilation. *Circulation*, 86(1):232–246.

Dvir, D., Kornowski, R., Gurevich, J., Orlov, B., and Aravot, D. (2003). Degrees of severe stenoses in sigma-shaped versus c-shaped right coronary arteries. *The American Journal of Cardiology*, 92(3):294–298.

Fischer, M., Mayer, B., Baessler, A., Riegger, G., Erdmann, J., Hengstenberg, C., and Schunkert, H. (2007). Familial aggregation of left main coronary artery disease and future risk

of coronary events in asymptomatic siblings of affected patients. *European Heart Journal*, 28(20):2432–2437.

Fiss, D. (2007). Normal coronary anatomy and anatomic variations. *Applied Radiology*, 36(1 SUPPL.):14–26.

Friedman, M. H., Deters, O. J., Mark, F. F., Bargeron, C. B., and Hutchins, G. M. (1983). Arterial geometry affects hemodynamics. a potential risk factor for athersoclerosis. *Atherosclerosis*, 46(2):225–231.

Glaunès, J., Qiu, A., Miller, M. I., and Younes, L. (2008). Large deformation diffeomorphic metric curve mapping. *International Journal of Computer Vision*, 80(3):317–336.

Ikeda, U., Kuroki, M., Ejiri, T., Hosoda, S., and Yaginuma, T. (1991). Stenotic lesions and the bifurcation angle of coronary arteries in the young. *Japanese Heart Journal*, 32(5):627–633.

Lorensen, W. E. and Cline, H. E. (1987). Marching cubes: A high resolution 3d surface construction algorithm. *Computer Graphics*, 21(4):163–169.

Loukas, M., Groat, C., Khangura, R., Owens, D. G., and Anderson, R. H. (2009). The normal and abnormal anatomy of the coronary arteries. *Clinical Anatomy*, 22(1):114–128.

McGill, Henry C, J., McMahan, C. A., and Gidding, S. S. (2008). Preventing heart disease in the 21st century: implications of the pathobiological determinants of atherosclerosis in youth (PDAY) study. *Circulation*, 117(9):1216–1227. PMID: 18316498.

Meng, S., Geyer, S. H., Viana, M. P., and Weninger, W. J. (2008). Objective characterization of the course of the parasellar internal carotid artery using mathematical tools. *Surgical and Radiologic Anatomy*, 30(6):519–526.

Mut, F., Wright, S., Ascoli, G. A., and Cebral, J. R. (2014). Morphometric, geographic, and territorial characterization of brain arterial trees. *International journal for numerical methods in biomedical engineering*.

O'Flynn, P. M., O'Sullivan, G., and Pandit, A. S. (2007). Methods for three-dimensional geometric characterization of the arterial vasculature. *Annals of Biomedical Engineering*, 35(8):1368–1381.

Piccinelli, M., Veneziani, A., Steinman, D. A., Remuzzi, A., and Antiga, L. (2009). A framework for geometric analysis of vascular structures: application to cerebral aneurysms. *IEEE transactions on medical imaging*, 28(8):1141–1155.

Roth, G. A., Forouzanfar, M. H., Moran, A. E., Barber, R., Nguyen, G., Feigin, V. L., Naghavi, M., Mensah, G. A., and Murray, C. J. (2015). Demographic and epidemiologic drivers of global cardiovascular mortality. *New England Journal of Medicine*, 372(14):1333–1341. PMID: 25830423.

Sun, Z. (2010). Multislice CT angiography in coronary artery disease: Technical developments, radiation dose and diagnostic value. *World Journal of Cardiology*, 2(10):333.

Thubrikar, M. J. and Robicsek, F. (1995). Pressure-induced arterial wall stress and atherosclerosis. *The Annals of Thoracic Surgery*, 59(6):1594–1603.

Whitaker, R. T. and Xue, X. (2001). Variable-conductance, level-set curvature for image denoising. In *Image Processing, 2001. Proceedings. 2001 International Conference on*, volume 3, pages 142–145. IEEE.

Wright, S. N., Kochunov, P., Mut, F., Bergamino, M., Brown, K. M., Mazziotta, J. C., Toga, A. W., Cebral, J. R., and Ascoli, G. A. (2013). Digital reconstruction and morphometric analysis of human brain arterial vasculature from magnetic resonance angiography. *NeuroImage*, 82:170–181.

Zhu, H., Ding, Z., Piana, R. N., Gehrig, T. R., and Friedman, M. H. (2009). Cataloguing the geometry of the human coronary arteries: A potential tool for predicting risk of coronary artery disease. *International Journal of Cardiology*, 135(1):43–52.